International Journal of Thermal Sciences 49 (2010) 1019–1025

Contents lists available at ScienceDirect

International Journal of Thermal Sciences

journal homepage: www.elsevier.com/locate/ijts

Thermoacoustic energy analysis of transverse-pin and tortuous stacks at large acoustic displacements

Konstantin I. Matveev*

School of Mechanical and Materials Engineering, Washington State University, Pullman, WA 99164-2920, USA

ARTICLE INFO

Article history:
Received 2 August 2009
Received in revised form
7 December 2009
Accepted 12 December 2009
Available online 13 January 2010

Keywords:
Heat–sound interactions
Thermoacoustics
Transverse-pin stack
Tortuous stack
Rayleigh's criterion
Lagrangian framework

ABSTRACT

A simplified method based on Rayleigh's criterion is developed for evaluating thermoacoustic power conversion in transverse-pin and tortuous stacks. Heat transfer and viscous losses are approximated by steady-flow correlations valid at large acoustic displacements with respect to a longitudinal pitch of a pin stack or a characteristic pore size of a random stack. A Lagrangian approach is employed to calculate temperature fluctuations of oscillating gas parcels inside the stack. A computational example is presented for a stack with an inline pin arrangement placed in a standing acoustic wave. Power conversion and efficiencies are evaluated for conditions relevant to a small-scale system. An indirect comparison is also made between theoretical results and experimental data for a prime mover with a wire mesh stack.

1. Introduction

Thermoacoustic engines generate sound from heat without moving solid parts. Acoustic modes inside the engine resonators become unstable if a sufficiently high-temperature gradient is imposed in a porous insert, known as stack, which should be properly positioned inside the system. A schematic of a simple standing-wave thermoacoustic prime mover is shown in Fig. 1. In-stack gas parcels undergoing motions in a fundamental acoustic mode receive heat from the stack in the moments of their compression and reject heat back to the stack in the rarefied states. Such a heat exchange transforms part of supplied heat into sound in accordance with Rayleigh's criterion [1]. Acoustic power produced in thermoacoustic engines can be used for a variety of applications [2], such as electricity generation and gas-mixture separation. A thermoacoustic device can also perform as a heat pump or refrigerator, if the temperature difference in the stack is sufficiently small and acoustic oscillations are imposed externally.

Low-amplitude thermoacoustic processes are well understood in stacks with longitudinal parallel-type geometries, where solid components of the stack are aligned in the direction of primary acoustic motions of gas particles [2]. Perhaps the most efficient longitudinal parallel-type configuration involves an array of pins [3], where convex solid surfaces increase thermoacoustic energy conversion while reducing viscous losses.

Stacks with non-uniform cross-sectional geometry comprise wire mesh screens [4], rigid foams [5,6], intermittent plate stacks [7], wools [8], and transverse-pin arrays [9]. Some of these stacks demonstrated a potential of higher performance in comparison with regular stacks that have longitudinal orientation of solid constituents. Another important advantage of non-uniform stacks is significantly reduced heat conduction leak through the stack solid matrix. However, thermoacoustic theories for such geometries are not well developed. Several important studies on thermoacoustics of non-uniform media include a harmonic analysis of stacked screen regenerators [10], measurements and correlations of heat transfer from wires near a thermoacoustic stack [11], and a capillary-tube modeling approach for random porous media [12].

The main objective of the present study is to develop a simplified analysis for thermoacoustic power conversion and the efficiency of this conversion in highly porous, relatively short stacks consisting of an array of pins oriented *perpendicular* to the main acoustic motion of gas. In analogy with the longitudinal pin arrangement, the convex surface of pins is expected to provide additional benefits in this configuration. An important limitation of the theory is that acoustic displacements of gas parcels must be much larger than a longitudinal distance between neighboring pins. In this regime, steady-flow correlations can be applied for

* Tel.: +1 509 335 1327; fax: +1 509 335 4662.
E-mail address: matveev@wsu.edu

1290-0729/$ – see front matter © 2009 Elsevier Masson SAS. All rights reserved.
doi:10.1016/j.ijthermalsci.2009.12.007

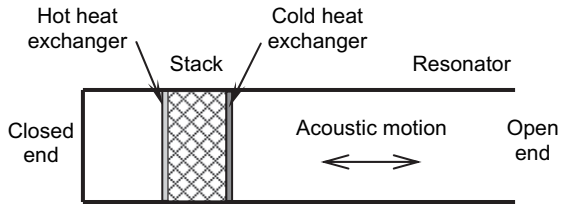

Fig. 1. Schematic of a standing-wave engine.

approximately estimating instantaneous heat transfer and viscous losses [2].

The theory presented here can be also used for high-displacement flow regimes in tortuous stacks if their steady-flow heat transfer and friction correlations are known. Such stacks are employed in miniature thermoacoustic devices [8,13]. A construction of regular-geometry stacks is challenging at small scales. Therefore, the availability of random porous stacks, such as made of reticulated vitreous carbon (RVC), is an important practical advantage, in addition to reduced heat conduction leak and good thermoacoustic performance.

2. Mathematical model

A porous stack with a length L_{st} much smaller than an acoustic wavelength λ is considered. An example of a transverse-pin stack arrangement is shown in Fig. 2. A constant gradient of the mean temperature dT_m/dx is imposed along the stack. The temperature difference between the stack ends, $L_{st}|dT_m/dx|$, is significantly smaller than the mean stack temperature $T_{st,m}$, which is used for evaluating gas properties. The gas inside the stack is represented by a row of moving gas slices (parcels) with fixed mass. Each parcel has a cross-sectional area of the stack and a thickness of one longitudinal pitch of the stack S_L (or characteristic pore size in a tortuous medium) evaluated at the parcel's mean temperature and pressure. The Lagrangian consideration employed here is similar to previous

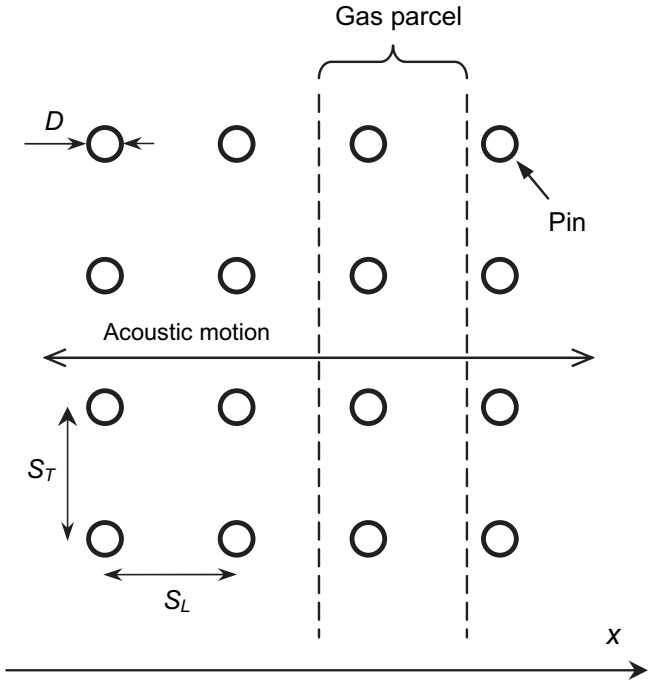

Fig. 2. Schematic of a small part of transverse-pin stack.

thermoacoustic analyses [14,15]. One-dimensional acoustic oscillations along the x-axis are present in the gas. The same acoustic pressure, velocity and displacement will approximate oscillations of all gas parcels inside a high-porosity short stack. Distortions of these parcels are neglected. The acoustic displacement x_1 should be much greater than S_L in order to use steady-flow heat transfer and friction correlations. At the same time, x_1 should be significantly smaller than the stack length L_{st} in order to minimize the influence of the stack ends.

Dynamics of one gas parcel is analyzed. Its acoustic velocity u', displacement x', and pressure fluctuation p' are described by the following equations,

$$u' = u_1 \sin\varphi, \tag{1}$$

$$x' = -x_1 \cos\varphi, \tag{2}$$

$$p' = p_1 \sin(\varphi + \theta), \tag{3}$$

where φ is the phase variable and θ is the phase shift between pressure and velocity fluctuations. The pressure amplitude is assumed to be relatively small in comparison with the mean pressure. It is also assumed that acoustic oscillations are monochromic, and the frequency of oscillations is determined by the resonator characteristics. The relation between acoustic pressure and velocity amplitudes depends on the stack position in the acoustic wave,

$$\frac{p_1}{u_1} = \rho_m a_m \overline{Z}, \tag{4}$$

where ρ_m and a_m are mean values of the gas density and the speed of sound, and $\overline{Z}$ is the absolute value of the non-dimensional specific acoustic impedance.

The evolution of the parcel temperature fluctuation in time (spatially averaged over the parcel) can be modeled as follows [14,15],

$$\frac{dT'}{d\varphi} = \frac{\gamma - 1}{\gamma} \frac{T_m}{p_m} \frac{dp'}{d\varphi} + \frac{1}{mc_p} \frac{dQ}{d\varphi}, \tag{5}$$

where γ is the specific heat ratio, T_m and p_m are the mean temperature and pressure of the gas parcel, m is the parcel mass, c_p is the specific heat at constant pressure, and Q is the heat addition to the parcel. The dominant causes for the gas-parcel temperature oscillations are pressure fluctuations and heat exchange with the stack. Contributions of heat conduction between gas parcels, heat generation due to viscous dissipation, and natural convection to the periodic temperature fluctuations are neglected.

Under the previously stated assumption $x_1 >> S_L$, it can be assumed that the heat transfer coefficient at each time moment depends on the instantaneous flow velocity in form of empirical steady-flow correlations [2,10]. Then, the following quasi-steady function for the convective heat transfer rate can be used,

$$\frac{dQ}{d\varphi} = -\frac{1}{\omega} h(|\mathrm{Re}(\varphi)|) A (T_g - T_s), \tag{6}$$

where ω is the angular acoustic frequency, h is the given steady heat transfer coefficient that depends on the instantaneous Reynolds number, system geometry, and gas properties; A is the reference area; T_g is the gas-parcel temperature; and T_s is the solid surface temperature. The heat transfer coefficient in Eq. (6) depends on the velocity magnitude but not on the frequency. This is in contrast to stacks with ideal longitudinal-pore geometries, where h depends on the frequency but not on the velocity magnitude [16]. In the longitudinal-pore configurations the gas region affected by heat

exchange with solid walls is correlated with the acoustic thermal penetration depth δ_k, which is a function of frequency [2]. The transverse-pin and tortuous stacks considered here are strongly non-uniform in the direction of acoustic oscillations. Hence, more intensive heat transport occurs in the transverse direction, making the heat transfer coefficient independent on the acoustic thermal penetration depth and dependent on the velocity magnitude at sufficiently high oscillation amplitudes [10,11].

A spatial variation of the stack mean temperature is assumed to be linear. Then, under the condition $x_1 >> S_L$, the solid temperature along the stack can be approximated as a linear function of x (rather than a stair-case function),

$$T_s \approx T_m + \frac{dT_m}{dx}x, \tag{7}$$

where dT_m/dx is the constant temperature gradient and x is the longitudinal coordinate, with $x = 0$ being the middle position of the gas parcel in a cycle. A solid material is assumed to have large heat capacity so that the solid temperature at a fixed location does not significantly change in time. The gas-parcel temperature can be presented as a sum of the mean and fluctuating parts,

$$T_g = T_m + T'(\varphi) \tag{8}$$

Substituting Eqs. (6–8) in Eq. (5) and numerically integrating Eq. (5), a periodic temperature fluctuation of the gas parcel can be found. A somewhat faster but less accurate calculation of the temperature fluctuation can be carried out by assuming that T' oscillates with the acoustic frequency and taking appropriate Fourier components of the heat transfer rate in Eq. (6).

Assuming similar temperature oscillations and heat transfer rate fluctuations for all in-stack gas parcels, the time-averaged thermoacoustic conversion of heat into acoustic power in the entire stack can be estimated using a quantitative form of Rayleigh's criterion [17],

$$\bar{\dot{E}}_{TA} = N\frac{\gamma-1}{\gamma p_m}\frac{\omega}{2\pi}\int_0^{2\pi}\frac{dQ}{d\varphi}p'd\varphi, \tag{9}$$

where $N = L_{st}/S_L$ is the number of gas parcels in the stack. Eq. (9) implies that heat addition to the gas must have a component oscillating in phase with the acoustic pressure in order to produce acoustic power. At a sufficiently small (or zero) temperature gradient in the stack, thermoacoustic power conversion (Eq. (9)) can be negative due to conventional thermal relaxation losses.

To account for acoustic damping due to viscous losses, a history-independent steady-flow correlation for the instantaneous pressure drop across the stack can be applied under the assumption $x_1 >> S_L$ [2,10],

$$\Delta p = \xi(|\mathrm{Re}(\varphi)|)\frac{\rho u'^2}{2}, \tag{10}$$

where ξ is the given coefficient of pressure drop that depends on the magnitude of instantaneous Reynolds number, stack geometry, and gas properties. The time-average viscous power loss is calculated as follows,

$$\bar{\dot{E}}_v = \frac{1}{2\pi}A_{st}\int_0^{2\pi}\Delta p|u'|d\varphi, \tag{11}$$

where A_{st} is the stack cross-sectional area. Scattering acoustic losses are neglected here since a pin diameter is much smaller than an acoustic wavelength.

Gas parcels oscillating in the stack carry heat either down or up the temperature gradient. This heat flow is due to hydrodynamic transport of entropy and can be estimated using the expression derived by Swift [18],

$$\bar{\dot{Q}}_t = \frac{1}{2\pi}A_{st}\rho_m c_p\int_0^{2\pi}T'u'd\varphi. \tag{12}$$

The temperature fluctuation in Eq. (12) should be evaluated at a fixed cross section in the stack, rather than at a gas parcel. However, under the assumptions of a short stack and a linear variation of the mean temperature, the integral in Eq. (12) calculated with either the parcel or point temperature will produce the same result. A direction of heat transport (or sign of $\bar{\dot{Q}}_t$) depends on whether a thermoacoustic system performs as a prime mover or a heat pump. We define $\bar{\dot{Q}}_t$ to be positive if heat is transported down the temperature gradient, i.e., the system works a prime mover. In a heat pump $\bar{\dot{Q}}_t < 0$, implying that heat is pumped up the temperature gradient. Since only high amplitudes of acoustic oscillations are considered, the heat conduction along the stack is relatively small and neglected in the current analysis, but it can be straightforwardly included.

The efficiency of acoustic energy generation inside a short stack with moderate temperature difference in a prime mover can be approximately calculated as follows,

$$\eta_{st} \approx \frac{\bar{\dot{E}}_{TA} - \bar{\dot{E}}_v}{\bar{\dot{Q}}_t} \tag{13}$$

The inviscid efficiency, $\eta_{st,in}$, which is sometimes used in the literature, can be calculated neglecting the viscous loss term in Eq. (13). The second-law efficiency is given by the expression,

$$\eta_{st,II} = \frac{\eta_{st}}{\eta_C} \approx \eta_{st}\frac{T_{st,m} + 0.5L_{st}|dT_m/dx|}{L_{st}|dT_m/dx|}, \tag{14}$$

where η_C is the Carnot efficiency. The Coefficient of Performance (COP) of a short stack in a thermoacoustic heat pump can be evaluated as follows,

$$\mathrm{COP}_{st} \approx \frac{-\bar{\dot{Q}}_t}{-\bar{\dot{E}}_{TA} + \bar{\dot{E}}_v}. \tag{15}$$

The minus signs in Eq. (15) account for the negative heat flow (up the temperature gradient) and negative thermoacoustic power conversion (acoustic losses) in a heat pump. It should be emphasized that efficiencies and COP defined here are stack-based. They do not account for losses that occur outside the stack, for example, at the resonator walls. Therefore, the overall system efficiencies will be smaller than the stack efficiencies.

3. Calculation results

3.1. Transverse-pin array stack

As an example of a transverse-pin stack, an inline array of pins is considered here (Fig. 2). The stack cross-sectional area is assumed to be a rectangle with breadth B and height H. The heat transfer coefficient of cylinders in the stack can be expressed via Nusselt number,

$$h = \frac{Nu\,k}{D}, \tag{16}$$

where k is the heat conduction coefficient in the gas and D is the pin diameter. Zukauskas [19] gives the empirical correlation for this configuration with a large number of tube rows in the steady flow and relatively small difference between temperatures of fluid and cylinders,

$$Nu = 0.9\mathrm{Pr}^{0.36}\mathrm{Re}_n^{0.4}, \tag{17}$$

where Pr is the Prandtl number, and $Re_n = \rho u_n D/\mu$ is based on the flow velocity in the narrowest section of the stack restrictions, which for the inline arrangement relates to flow velocity outside restrictions as follows,

$$u_n = u' \frac{S_T}{S_T - D}, \tag{18}$$

where S_T is the vertical pitch (Fig. 2). Eq. (17) is valid for Reynolds numbers between 1 and 100. The occurrence of $Re_n < 1$ during an acoustic cycle does not significantly affect variation of the heat transfer rate, if the maximum Reynolds number (based on the velocity amplitude) is much higher than one. The reference area A in Eq. (6) is the total surface area of cylinders in one vertical row,

$$A = \pi D B \frac{S_T}{H}. \tag{19}$$

An empirical expression for the pressure drop in an inline bank of tubes is obtained by Gaddis and Gnielinski [20],

$$\Delta p = N \frac{f_a}{\mathrm{Re}_n} \frac{\rho u_n^2}{2}, \tag{20}$$

where $N = L_{st}/S_L >> 1$ is the number of cylinders in the horizontal direction, index n stands for the narrowest section in the stack, and f_a is the arrangement factor given as follows,

$$f = \frac{280\pi\left[\left(S_L^{0.5}/D^{0.5} - 0.6\right)^2 + 0.75\right]}{\left(4 S_L S_T/D^2 - \pi\right)(S_T/D)^{1.6}}. \tag{21}$$

The range of application of Eqs. (20) and (21) is the same as for the heat transfer coefficient (Eq. (17)).

For sample calculations, stack parameters appropriate for a small-scale thermoacoustic system are considered. The stack length is 7 mm, and the stack cross-sectional area is 1 cm^2. The pin diameter is 0.05 mm and $S_L/D = S_T/D = 3$. The atmospheric air serves as a working fluid. Properties are evaluated at the mean stack temperature of 400 K. The standing-wave condition is chosen here, corresponding to $\theta = \pi/2$ in Eq. (3), and $\overline{Z}$ in Eq. (4) is selected to be 5, as recommended for standing-wave devices [21]. The acoustic frequency is 1 kHz. The acoustic displacement x_1 is a variable parameter in the range $5 < x_1/S_L < 15$.

Two different operational regimes, corresponding to the prime mover and heat pump modes, are considered here. It is known that the thermoacoustic energy conversion (Eq. (9)) is positive only if the mean temperature gradient in the stack exceeds a certain threshold. For an inviscid ideal gas in the standing wave near a single plate, this threshold, known as the ideal critical temperature gradient, was derived by Swift [18],

$$\left(\frac{dT_{crit}}{dx}\right)_{id} = -\frac{a\omega}{c_p}\overline{Z}. \tag{22}$$

For the selected system properties, the ideal critical temperature gradient is about −125 K/cm. The temperature gradient must be negative due to a selection of positive phase shift between pressure and velocity fluctuations. The commonly used ratio of the actual temperature gradient to the ideal gradient is defined as follows,

$$\Gamma = \frac{dT}{dx} \Big/ \left(\frac{dT_{crit}}{dx}\right)_{id}. \tag{23}$$

If $\Gamma > 1$, then a system can produce acoustic power; with $\Gamma < 1$ and imposed acoustic oscillations, the system can pump heat up the temperature gradient. In the present example, Γ is selected to be 1.5 (engine) and 0.5 (heat pump).

The calculated temperature fluctuation of a gas parcel in a cycle at $\Gamma = 1.5$ and $x_1 = 10 S_L$ is presented in Fig. 3a. Also shown in the figure are the smoothed temperature variation of the solid stack on the particle path, $T_s' = T_s - T_m$, and the isentropic acoustic temperature fluctuation which is defined as follows,

$$T_{ac} = \frac{\gamma - 1}{\gamma} \frac{T_m}{p_m} p'. \tag{24}$$

The behavior of the gas-parcel temperature fluctuation can be associated with the form of Eq. (5). Pressure oscillations cause gas temperature fluctuations to be similar to those in any acoustic wave. In the absence of the stack, the gas temperature oscillations would be given by Eq. (24). On the other hand, in case of infinitely large heat transfer coefficient, the gas temperature would be equal to the local solid-stack temperature T_s. When the pressure-induced and heat-induced effects are comparable, the gas temperature oscillates with some phase shift with respect to both T_{ac} and T_s', because of the presence of velocity fluctuation in the heat transfer coefficient which is phase-shifted relative to pressure oscillations.

The instantaneous rate of heat addition to the gas parcel is shown in Fig. 3b. Its sign depends on the temperature difference between gas and solid, while the magnitude also depends on the instantaneous velocity. The product of heat addition rate and pressure fluctuation, which is also given in Fig. 3b, is of the most importance for thermoacoustic energy conversion. For sufficiently large magnitude of the mean temperature gradient, the integral of $p' dQ/d\varphi$ over a cycle is greater than zero, corresponding to a positive thermoacoustic power conversion (Eq. (9)) or sound

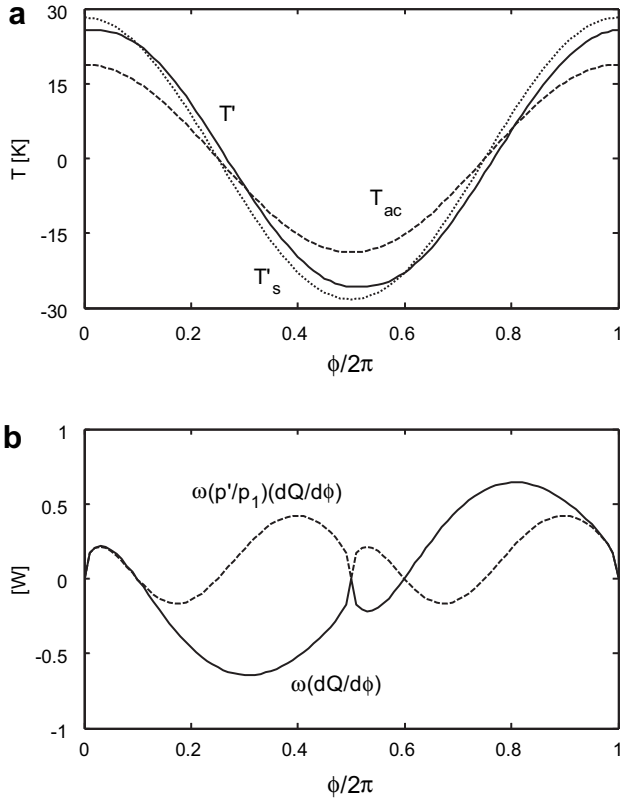

Fig. 3. Time dependence of gas-parcel properties during one acoustic cycle at $x_1/S_L = 10$ and $\Gamma = 1.5$. (a) Solid line, parcel temperature fluctuation; dashed line, acoustic temperature fluctuation, dotted line, smoothed temperature variation of the solid matrix on the gas-parcel path. (b) Solid line, heat transfer rate to the gas parcel; dashed line, product of heat transfer rate and non-dimensional pressure fluctuation.

production from heat. If a magnitude of the mean temperature gradient is smaller than a threshold value, then unsteady heat addition to the gas would lead to sound attenuation.

For the variable acoustic displacement with other parameters fixed, the corresponding Reynolds number based on the amplitude of acoustic velocity and the relative pressure amplitude are shown in Fig. 4. Reynolds numbers are in the range valid for heat transfer and pressure drop correlations (Eqs. (17) and (20)), while the pressure amplitude corresponds to a high-amplitude operational range of thermoacoustic devices.

Calculation results for the time-average acoustic power generation, viscous losses, and heat flow along the prime-mover stack are shown in Fig. 5a. All power values, including the useful power $\dot{E}_{TA} - \dot{E}_v$, increase with increasing displacement amplitude. Corresponding efficiencies are plotted in Fig. 5b. The calculated inviscid efficiency, $\eta_{st,in} \sim 0.26$, exceeds the inviscid thermoacoustic efficiency of a single flat plate ($\sim$0.19) evaluated in similar conditions [18]. The viscous losses in the flow around pins reduce the actual stack-based efficiency η_{st} down to about 0.1, which corresponds to the second-law efficiency of around 0.4.

Powers and efficiencies of the same stack operating as a heat pump at $\Gamma = 0.5$ are shown in Fig. 6. The heat transported to a high-temperature sink and acoustic losses increase with the gas displacement. The inviscid and viscous COP are around 3 and 5.5, respectively; while the reversible COP is about 9.6 at the given conditions. This makes the second-law efficiency of the stack with viscous losses around 0.3.

Additional losses in resonators and heat exchangers will further reduce the overall system efficiency. However, no optimization has been performed in the present study. Variations in the gas type, mean pressure, and system geometry may lead to significant efficiency gains. Such an optimization will also require knowledge of needed specifications and possible constrains of a thermoacoustic device.

We are aware of only one set of thermoacoustic measurements with transverse-pin stacks that were carried out by Petculescu [9]. However, no comparison can be made with our modeling since those experiments were conducted at low acoustic amplitudes beyond the applicability range of the present theory.

3.2. Prime mover with wire mesh stack

Some experimental data are available for a prime mover with a wire mesh stack [4]. However, the stack characteristics in this case can be analyzed only through the entire system performance which is reported in [4]. This will require making additional simplifications in the acoustical analysis for the system outside the stack.

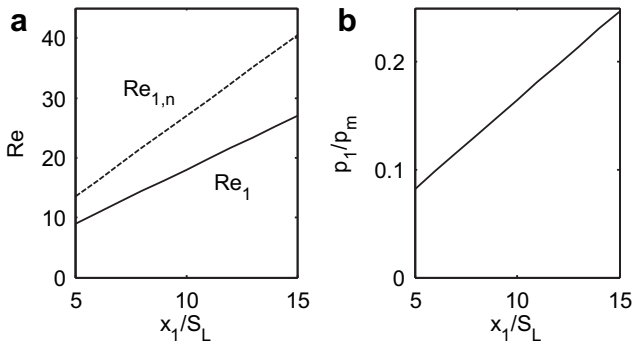

Fig. 4. (a) Reynolds numbers based on the velocity amplitudes: solid line, outside restrictions; dashed line, in the narrowest stack sections. (b) Relative pressure amplitude.

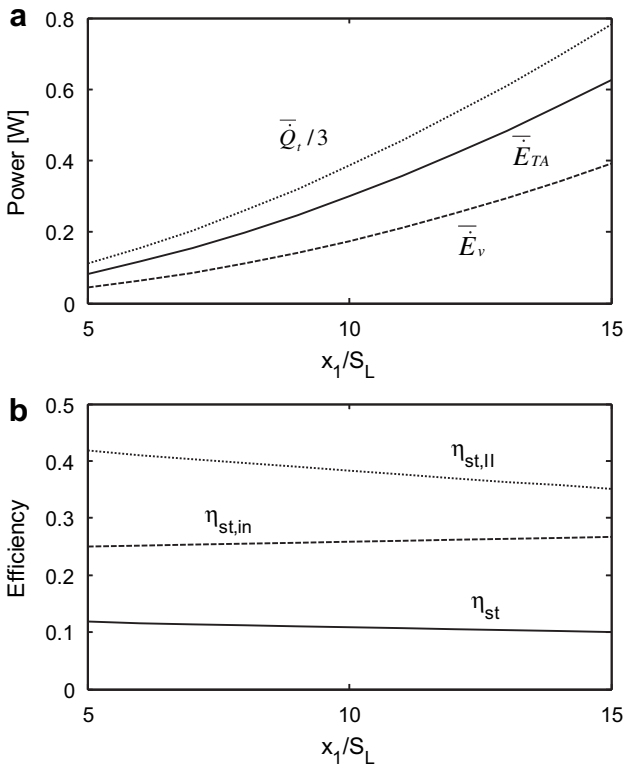

Fig. 5. Calculated stack performance in the prime mover mode; $\Gamma = 1.5$. (a) Solid line, thermoacoustic power conversion; dashed line, viscous power loss; dotted line, heat flow (divided by 3). (b) Solid line, stack efficiency; dashed line, inviscid efficiency; dotted line, second-law efficiency.

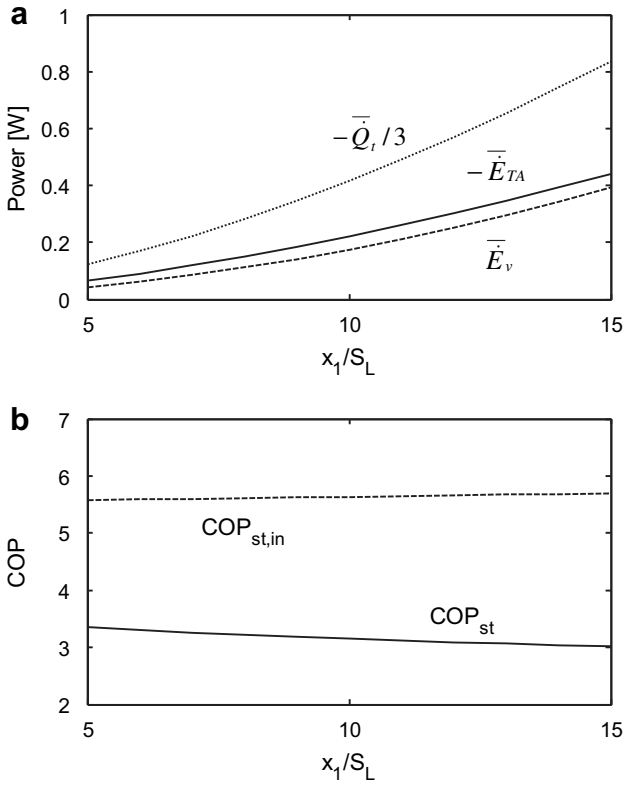

Fig. 6. Calculated stack performance in the heat pump mode; $\Gamma = 0.5$. (a) Solid line, thermoacoustic power conversion; dashed line, viscous power loss; dotted line, heat flow (divided by 3). (b) Solid line, stack COP; dashed line, inviscid COP.

Also, a large stack temperature difference was present in experiments, comparable with an absolute temperature. These factors imply that only indirect and qualitative comparison can be made with the theory developed in this paper.

A quarter-wavelength thermoacoustic engine, similar in principle to that shown in Fig. 1, was driven by a temperature difference produced by cooling the open-ended resonator part by liquid nitrogen. The resonator length and radius were 28.6 cm and 1.9 cm, respectively. A 1.4-cm-long stack was positioned at about 11.4 cm from the closed end. Randomly oriented wire meshes were used as the stack material. Heat exchangers on both sides of the stack were made from parallel copper fins [22]. The sound generated by the system was measured in the anechoic chamber by a microphone located half meter away from the open tube end. The first fifty quasi-steady-state acoustic cycles were used for measurements. The voltage signal reported in [4] is converted to the acoustic pressure using the microphone sensitivity also cited in [4]. The experimentally measured RMS pressure for setups with stacks made of standard mesh screens is shown as a function of the stack porosity ψ in Fig. 7.

To make a comparison with these results, we expand a simplified energy balance method for a standing-wave thermoacoustic engine proposed by Swift [18] and include acoustic losses important at high amplitudes of acoustic oscillations. In the steady-state, the time-average acoustic power generated in the stack is balanced by acoustic damping mechanisms,

$$\bar{\dot{E}}_{TA} = \bar{\dot{E}}_{v} + \bar{\dot{E}}_{res} + \bar{\dot{E}}_{hx} + \bar{\dot{E}}_{ml} + \bar{\dot{E}}_{rad} + \bar{\dot{E}}_{end}, \tag{25}$$

where $\bar{\dot{E}}_{TA}$ and $\bar{\dot{E}}_{v}$ are time-averaged thermoacoustic power production and viscous losses inside the stack given by Eqs. (9) and (11). The steady-flow friction and heat transfer coefficients were obtained from empirical data of Kays and London [23]. All other terms in Eq. (25) are explained below.

The thermoviscous losses at the resonator walls and surfaces of a single heat exchanger are evaluated using standard expressions [18],

$$\bar{\dot{E}}_{res} = \frac{1}{4}\frac{P_A^2}{\rho_m a_m^2}\omega\pi R_{res}L_{res}\left[\delta_k(\gamma-1)\left(1+\frac{R_{res}}{L_{res}}\right)+\delta_v\right], \tag{26}$$

$$\bar{\dot{E}}_{hx,0} = \frac{1}{4}A_{hx}\omega\left[\frac{p_1^2}{\rho_m a_m^2}\delta_k(\gamma-1)+\rho_m u_1^2\delta_k\right], \tag{27}$$

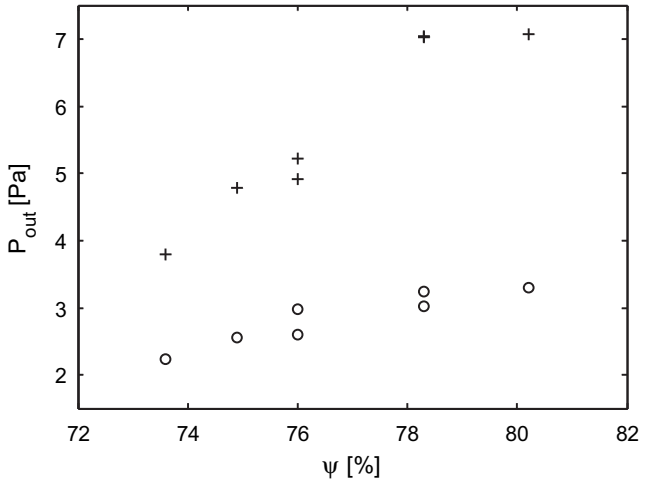

Fig. 7. RMS acoustic pressure outside the prime mover. Circles, test data [4]; crosses, calculated results.

where P_A is the acoustic pressure amplitude at the closed end, R_{res} is the resonator radius, L_{res} is the resonator length, $\delta_v = \sqrt{2\mu/\rho\omega}$ is the viscous penetration depth, μ is the fluid viscosity, $\delta_k = \sqrt{2k/\rho c_p\omega}$ is the thermal penetration depth, k is the fluid heat conductivity. In Eq. (27), p_1 and u_1 are the acoustic pressure and velocity evaluated at the positions of heat exchangers. The fundamental acoustic waveforms are also assumed using the average-temperature approximation in an ideal resonator [18],

$$p_1(x) = P_A\cos\left(2\pi\frac{x}{\lambda}\right), \tag{28}$$

$$u_1(x) = \frac{P_A}{\rho_m a_m}\sin\left(2\pi\frac{x}{\lambda}\right). \tag{29}$$

Inside the stack and heat exchangers, the velocity given by Eq. (29) should be divided by porosity of a corresponding element to obtain an actual acoustic velocity. The minor loss at one side of a heat exchanger is calculated as follows [2],

$$\bar{\dot{E}}_{ml,0} = \frac{2}{3}K\rho_m R_{res}^2 u_1, \tag{30}$$

where K is the minor loss coefficient that depends on the open area ratio [24].

The sound radiation term is given by the formula [18],

$$\bar{\dot{E}}_{rad} = \frac{\pi^3}{2}\frac{P_A^2 R_{res}^4}{\rho_m a_m \lambda^2}. \tag{31}$$

At high acoustic amplitudes, there are additional losses at the open end of the resonator. Using results of Chester [25], Heckl [26] related these losses to $\bar{\dot{E}}_{rad}$ as follows,

$$\bar{\dot{E}}_{end} \approx \bar{\dot{E}}_{rad}\frac{4}{\pi}\frac{a_m u_1}{(\omega R_{res})^2}, \tag{32}$$

where the acoustic velocity amplitude is evaluated at the open end of the resonator.

The energy balance expressed by Eq. (25) allows us to determine the equilibrium pressure amplitude inside the resonator, since other parameters are known. Then, the acoustic power radiated from the open end is determined. For approximate estimations, spherical spreading can be assumed [27]. The RMS acoustic pressure outside the engine at a distance s from the open end can be found as follows [28],

$$P_{out} = \sqrt{\frac{\bar{\dot{E}}_{rad}\rho a}{4\pi s^2}}, \tag{33}$$

where ρ and a are the density of the media (air) outside the engine.

Calculations are carried out for conditions similar to experimental, i.e., using the same stated porosity, mesh size, number of screens, wire diameter, temperature difference, and frequency. The computed RMS acoustic pressure at the microphone location is presented in Fig. 7. The pressure magnitude increases with increasing the stack porosity as in the test data. However, the pressure amplitude is significantly over-predicted. One of the possible causes is a large uncertainty in the stack porosity. Screens were tightly packed under a force, so the formal porosity given in [4] as for an array of crossed straight rods is likely to overestimate the actual porosity. Results in Fig. 7 suggest that lower porosity values would result in smaller calculated pressure amplitudes closer to experimental data. Nevertheless, even a factor-of-two agreement can be considered satisfactory given the simplified analysis of the prime mover and unknown experimental uncertainties. More accurate high-amplitude experiments specifically

addressing thermoacoustic properties of tortuous stacks are needed for the theory validation.

4. Concluding remarks

A simplified model based on steady-flow correlations, Lagrangian approach, and Rayleigh's criterion has been developed for thermoacoustic analysis of short transverse-pin stacks with moderate temperature differences. This method provides fast estimations for thermoacoustic power conversion and the efficiency of this process. The model is subject to several limitations, including a requirement of having a large acoustic displacement relative to a longitudinal spacing between pins. This theory can be also applied to tortuous stacks but requires knowledge of corresponding steady-flow heat transfer and flow resistance correlations. A calculation example demonstrated reasonably good (for small-scale systems) performance of a transverse-pin stack. A qualitative correlation was found between the model results and test data for a prime mover with a wire mesh stack. Future theoretical developments can address relaxing some of the model assumptions, such as a relation of the acoustic displacement to the stack length and pore size, while retaining the model simplicity for fast calculations.

Acknowledgements

This work is supported by the NSF Thermal Transport Processes Program under Grant No. 0853171.

References

[1] J.W.S. Rayleigh, The Theory of Sound. Dover Publications, New York, 1945.
[2] G.W. Swift, Thermoacoustics: a Unifying Perspective for Some Engines and Refrigerators. Acoustical Society of America, Sewickley, PA, USA, 2002.
[3] G.W. Swift, R.M. Keolian, Thermoacoustics in pin-array stacks. J. Acoust. Soc. Am. 94 (1993) 941–943.
[4] M.S. Reed, Measurements with wire mesh stacks in thermoacoustic prime movers, M.S. thesis, Naval Postgraduate School, Monterey, CA, USA, 1996.
[5] J.A. Adeff, T.J. Hofler, A.A. Atchley, W.C. Moss, Measurements with reticulated vitreous carbon stacks in thermoacoustic prime movers and refrigerators. J. Acoust. Soc. Am. 104 (1998) 32–38.
[6] G. Petculescu, L. Wilen, Lumped-element technique for the measurement of complex density. J. Acoust. Soc. Am. 110 (2001) 1950–1957.
[7] J. Bosel, Ch. Trepp, J.G. Fourie, An alternative stack arrangement for thermoacoustic heat pumps and refrigerators. J. Acoust. Soc. Am. 106 (1999) 707–715.
[8] O.G. Symko, E. Abdel-Rahman, Y.S. Kwon, M. Emmi, R. Behunin, Design and development of high-frequency thermoacoustic engines for thermal management in microelectronics. Microelectronics J. 35 (2004) 185–191.
[9] G. Petculescu, Fundamental measurements in standing-wave and traveling-wave thermoacoustics, Ph.D. thesis, Ohio University, Athens, OH, USA, 2002.
[10] G.W. Swift, W.C. Ward, Simple harmonic analysis of regenerators. J. Thermophys. Heat Transfer 10 (1996) 652–662.
[11] G. Mozurkewich, Heat transfer from transverse tubes adjacent to a thermoacoustic stack. J. Acoust. Soc. Am. 110 (2001) 841–847.
[12] H.S. Roh, R. Raspet, H.E. Bass, Parallel capillary-tube-based extension of thermoacoustic theory for random porous media. J. Acoust. Soc. Am. 121 (2007) 1413–1422.
[13] K.I. Matveev, N. Shafiei-Tehrany, C.D. Richards, Small-scale thermoacoustic engine demonstrator, in: Proceedings of 8th International workshop on micro and nanotechnology for power generation and energy conversion applications, Sendai, Japan, 2008.
[14] R.S. Wakeland, R.M. Keolian, Calculated effects of pressure-driven temperature oscillations on heat exchangers in thermoacoustic devices with and without a stack. J. Acoust. Soc. Am. 116 (2004) 294–302.
[15] K.I. Matveev, G.W. Swift, S. Backhaus, Temperatures near the interface between an ideal heat exchanger and a thermal buffer tube or pulse tube. Int. J. Heat Mass Transf. 49 (2006) 868–878.
[16] J. Liu, S.L. Garrett, Relationship between Nusselt number and the thermo-viscous (Rott) functions. J. Acoust. Soc. Am. 119 (2006) 1457–1462.
[17] F.E.C. Culick, A note on Rayleigh's criterion. Combust. Sci. Technol. 56 (1987) 159–166.
[18] G.W. Swift, Thermoacoustic engines. J. Acoust. Soc. Am. 84 (1988) 1145–1180.
[19] A. Zukauskas, Convective heat transfer in cross flow. in: S. Kakac, R.K. Shah, W. Aung (Eds.), Handbook of Single-Phase Convective Heat Transfer. Wiley, New York, 1987 (Chapter 6).
[20] E.S. Gaddis, V. Gnielinski, Pressure drop in cross flow across tube bundles. Int. Chem. Eng. 25 (1985) 1–15.
[21] S. Backhaus, G.W. Swift, New varieties of thermoacoustic engines, in: Proceedings of 9th International congress on sound and vibration, Orlando, FL, USA, 2002.
[22] J.A. Adeff, Measurement of the space thermoacoustic refrigerator performance, M.S. thesis, Naval Postgraduate School, Monterey, CA, USA, 1990.
[23] W.M. Kays, A.L. London, Compact Heat Exchangers. McGraw-Hill, New York, 1964.
[24] R.W. Fox, A.T. McDonald, Introduction to Fluid Mechanics. Wiley, 1985.
[25] W. Chester, Resonant oscillations of a gas in an open-ended tube. Proc. Royal Soc. A 337 (1981) 449–467.
[26] M.A. Heckl, Non-linear acoustic effects in the Rijke tube. Acustica 72 (1990) 63–71.
[27] S.L. Garrett, Acoustic laser kit instructions, Penn State, State College, PA, USA, 2001.
[28] D.T. Blackstock, Fundamentals of Physical Acoustics. Wiley, New York, 2000.